Sustainable Energy, Grids and Networks 42 (2025) 101709

Contents lists available at ScienceDirect

Sustainable Energy, Grids and Networks

journal homepage: www.elsevier.com/locate/segan

Simultaneous planning of distribution automation and battery energy storage systems for improving resilience of distribution network

Mohammad Sadeghian-Jahromi [a], Mahmud Fotuhi-Firuzabad [b], Sajjad Fattaheian-Dehkordi [a,*], Fei Wang [c], Matti Lehtonen [a]

[a] *Department of Electrical Engineering and Automation, Aalto University, Espoo, Finland*
[b] *Department of Electrical Engineering, Sharif University of Technology, Tehran, Iran*
[c] *Department of Electrical Engineering, North China Electric Power University, Boading, China*

ARTICLE INFO

Keywords:
Reliability
Resilience
Distribution network
Simultaneous planning
Distribution automation
Battery energy storage systems
Remote control switches
Automation control
Stochastic Programming
Distribution system optimization

ABSTRACT

Recent widespread blackouts around the world have highlighted the fact that power grids must not only ensure reliability against high-probability, low-impact events (HPLI), but also withstand against low-probability, high-impact events (HILP) which could endanger the reliable operation of the system. Therefore, with the aim of improving the resilience of distribution networks, this paper proposes a model for the simultaneous planning of distribution automation and energy storage systems to address the operational challenges in case of hurricane occurrences in the system. For this, first, a hurricane model is presented to predict the impact of future hurricanes on the network. Respectively, the planning optimization is formulated as a mixed integer linear programming (MILP) to optimally determine the location and number of the remote-control switches (RCSs) as well as the capacity, number and location of the battery energy storage systems (BESSs). This study enables the co-optimization of distribution automation and energy storages investments to effectively improve the resilience of the system. Finally, this model is implemented on the Roy Billinton Test System (RBTS) to investigate the effectiveness of the proposed method in improving the resilience of system in an economic manner.

1. Introduction

Resilience is defined as the system's ability to maintain an acceptable level of performance against an extreme event and recover within a reasonable period of time [1]. The occurrence of adverse weather conditions and natural disasters has always led to massive losses and blackouts at the level of distribution networks, which could be a challenging condition as the number and intensity of these events have been increasing due to climate changes in recent years [2].

In 2003, large parts of the United States and Canada experienced several days of power outages. This outage, which was caused by falling of trees on power lines, caused a loss between 4 and 10 billion dollars and about 50 million people faced power outages [3]. In 2012, during Hurricane Sandy, the economic damage was between 14 and 60 billion dollars [4], and the significant point in this event was the destruction of other electricity dependent infrastructures such as the water supply infrastructures [5]. This incident proved the importance of electricity infrastructure as the main and vital infrastructure of the country. In 2017, hurricanes Harvey, Irma, and Maria caused power outages that resulted in an estimated economic loss of $202 billion in the United States [6]. Also, a comparison between the causes of large blackouts in the United States has been made in [7]. This comparison clearly shows how the hurricane has the most impact among the various events that have caused extensive blackouts.

In response to the increasing scale and severity of disturbances, electricity utilities have started to improve the infrastructure in the power system. Respectively, most of the measures are aimed at preventing disturbances or increasing the level of protection of the system [8]. Resilience improvement measures are usually classified into three parts: hardening, planning, and operation. For example, authors in [9] recommend the use of underground cables instead of overhead lines to improve resilience against strong winds or hurricanes. According to [10], a higher substation level than the flood level is a suitable measure to improve resilience against floods. Reference [11] presents a robust optimal line hardening approach with multiple temporary microgrids to increase the resilience of distribution networks. In the context of planning and operation measures, [12] has presented a stochastic planning model considering distributed generators and network reconfiguration to improve the resilience of the distribution network. In order to

* Corresponding author.
E-mail address: sajjad.fattaheiandehkordi@aalto.fi (S. Fattaheian-Dehkordi).

https://doi.org/10.1016/j.segan.2025.101709
Received 24 September 2024; Received in revised form 22 March 2025; Accepted 30 March 2025
Available online 5 April 2025

Nomenclature

Sets and Indices

u	index of network generators
l	index of lines
n	index of buses
s	index of hurricane scenarios
t	index of time steps
h	index of candidate locations for RCS placement
f	index of network feeders
$\varnothing$	null set

Parameters

C_{BESS}^{f}	fixed installation and investment cost of BESS ($)
C_{P}^{BESS}	variable investment cost of BESS related to power capacity ($/MW)
C_{E}^{BESS}	variable investment cost of BESS related to energy Capacity ($/MWh)
C_{sw}^{f}	fixed installation and investment cost of RCSs ($)
P_{n}^{D}	active power demands at bus n
$AC_{f,l,n}$	determines the upstream bus $n$corresponding to each line $l$of feeder f
$BC_{f,l,n}$	determines the downstream bus $n$corresponding to each line $\boldsymbol{l}$ of feeder f
$b_{f,l}$	susceptance for each line $l$of feeder f
M	satisfactorily large positive number
$cap_{f,l}$	capacity for each line $l$of feeder f
cap_{u}^{G}	maximum active power outputs of generator u
η_{d}	discharge efficiency of each BESS
∂	the self-discharging rate of the battery
SOC_{n}^{max}	maximum fixed capacity for each BESS
TH	planning time horizon
$d_{f,s,t}^{1}$	number of the first outage line from feeder f, at time t of scenario s
$d_{f,s,t}^{2}$	number of the second outage line from feeder f, at time t of scenario s
$pr(s)$	probability of each scenario s
$CDF_{n,t}^{RE}$	customer damage function for each type of load and in each time step
cdf^{total}	total allowed customer damage determining the resilience level
$N_{\max}^{BESS}$	maximum number of BESS allowed to schedule
$N_{\max}^{sw}$	maximum number of RCSs allowed to schedule
$Budget$	budget limit
$P_{u}^{G,\max}$	Maximum power from main grid

Variables

$NESS(n)$	binary variable with 1 representing the BESS located in bus $n$and 0, otherwise
$P_{max}^{BESS}(n)$	maximum active power outputs of BESS
$E_{max}^{BESS}(n)$	maximum energy outputs of BESS
$N_{f,h}^{sw}$	binary variable with 1 representing the RCSs located in candidate location h of feeder f and 0, otherwise
$P_{u,s,t}^{G}$	active power outputs of generator $u$in scenario $s$at time t
$P_{n,s,t}^{LC}$	active load curtailment at bus $n$in scenario s at time t
$P_{n,s,t}^{BESS}$	active power outputs of BESS at bus $\boldsymbol{n}$ in scenario s at time t
$Pf_{f,l,s,t}^{s}$	sending active power flow across line $l$of feeder f in scenario s at time t
$Pf_{f,l,s,t}^{r}$	receiving active power flow across line $l$of feeder f in scenario s at time t
$\delta_{n,s,t}$	bus $n$voltage angle in scenario s at time t
$\vartheta_{f,l,s,t}$	binary variable with 0 representing line $l$of feeder $\boldsymbol{f}$ in scenario $\boldsymbol{s}$ at time $t$is closed and 1 otherwise
$SOC_{n,s,t}$	energy level of BESS at bus $n$in scenario s at time $\boldsymbol{t}$
$\vartheta_{f,l,s,t}^{1}$	auxiliary binary variable with 0 representing line $l$of feeder f in scenario s at time $t$is isolated from upstream fault and 1, otherwise
$\vartheta_{f,l,s,t}^{2}$	auxiliary binary variable with 0 representing line $l$of feeder f in scenario s at time $t$is isolated from downstream fault and 1, otherwise

improve the resiliency of an unbalanced distribution network, tie-line planning is proposed in [13]. Also, in [14], microgrid planning is used to have a resilient distribution network. Moreover, [15] presents an approach for the simultaneous expansion planning of transmission and sub-transmission networks. Simultaneous planning of interruptible loads, renewable generations, and capacitors in a distribution network, as well as providing an optimization approach for simultaneous planning of distributed generations and reconfiguration of the distribution network are studied in [16] and [17], respectively. In addition, a decentralized risk-constrained model has been introduced in [18] utilizing the ADMM algorithm to enhance the resilience of both power distribution system and natural gas system through enhancing energy sharing during flood. Also, due to the importance of electricity and gas infrastructures and their impact on each other, a resilience assessment considering both infrastructures under extreme weather conditions has been done in [19], although no solution to improve resilience has been provided. A microgrid-based operational framework is introduced in [20] to investigate the role of microgrids in improving the resilience of power systems against extreme events. This is despite the fact that none of these have been planned to make the network resilient against the hurricane. In the field of improving resilience against hurricane, a new resilience index has been defined in [4] while upgrading distribution poles as well as distributed generation (DG) placement has been used to improve resilience.

Meanwhile, nowadays, the smartening of the power system is one of the most important emerging technologies to control generation and demand, fast fault detection, and quick restoration [21]. One of the proposed solutions to improve resilience is the application of smart grid technology and particularly distribution automation, which makes it possible to perform tasks automatically. In fact, distribution automation improves the level of resilience and reliability by reducing the downtime of customers [22,23]. Due to the fact that it is not possible to perform switching operations during extreme events such as hurricanes, distribution automation provides the possibility of isolating and reconfiguring the network [23]. The importance of network reconfiguration is also emphasized in [24] and some references for reconfiguration schemes using remote control switches are introduced, but neither a model nor a reference for the optimal placement of remote switches is provided. The formation of automatic microgrids [25], optimal placement of switches [26] and optimal planning of fault management operations [27] are among other tasks performed in the field of distribution automation. In these studies, planning has been done to improve reliability, but there is room to present a model for planning to improve resilience.

Although the use of energy storage can be a solution to improve resilience, few studies have analyzed this issue [28,29]. Reference [30] presents a resilience-based design approach for battery energy storage systems (BESS) in advanced distribution networks. By introducing the concept of transportable energy storage systems (TESSs) in [31], it is shown that the resilience of the distribution system is improved with portable energy storage systems compared to conventional energy storage systems. In fact, the majority of existing works in this field highlight the central role of using energy storage systems in improving resilience, which is expected to become a strong competitor against other distributed energy resources in the coming years.

Determination of optimal location and number of switches in a distribution network from different perspectives has been studied, but no detailed studies have been done to plan switches for resilience improvement of the network. Although in [32], the planning of switches has been done by providing the resilience criterion as the objective function, but only up to two simultaneous outages have been considered in the network. In the case of extreme events such as hurricanes, a large number of lines in a network's feeder may fail. Also, the model presented in [32] has not considered the characteristics of the hurricane and the time-based nature of the hurricane scenarios.

In the field of BESS, [33] has made a plan to find the location and size of battery storages by providing the resilience criterion as the objective function. This planning problem is aimed at improving resilience against earthquakes. Nevertheless, this work did not study the planning of BESSs for resilience improvement against hurricanes as an event that has caused more damage to the power grid compared to other events in the world [34]. It is worth mentioning that the planning to improve resilience against hurricane is significantly different from the network planning to improve resilience against other events such as earthquake. In addition, the network outage scenarios occur simultaneously in an earthquake event while in a hurricane event, the outage scenarios occur at different times. Therefore, this makes it impossible to use the model presented in [33] to study a hurricane event. Also, the proposed model in [33] has been done on an isolated system from the main network. Table 1 presents a comprehensive taxonomy table of research works in the context of this paper. The main contributions of this paper are summarized as follows:

(1) Presenting a model for distribution automation planning in order to improve resilience against hurricanes by considering hurricane characteristics and the time-based nature of scenarios, which has not been studied in detail in literature.
(2) Presenting a model for planning battery energy storage systems to improve hurricane resilience, while taking into account the time-based nature of hurricane scenarios. In this regard, a general hurricane model is utilized to capture the uncertainties associated with hurricane's impacts on the grid.
(3) Proposing an optimization model for the simultaneous planning of distribution automation and battery energy storages by considering the constraints and different cases in order to improve grid resilience, which has not been conducted in previous research studies.

Based on the above discussions, the simultaneous planning of automation system and energy storages in a distribution system to improve its resilience in case of hurricane occurrences has not yet been fully studied. Respectively, in this study, a hurricane model is first presented that predicts future hurricanes and their impacts on the network. Then, a model for simultaneous planning of distribution automation and energy storage systems in order to improve resilience is developed. As a result of implementing this approach, the optimal number and location of remote-

control switches (RCSs) as well as the number, location, and size of battery energy storages are determined. Finally, the effectiveness of the proposed model will be evaluated by implementing it on a test network.

This paper is structured as follows. In Section 2, an overview of the planning model is discussed, followed by the hurricane hazard modeling in Section 3. Moreover, the optimization formulation for system planning is presented in Section 4. Finally, the effectiveness of the proposed model is evaluated by implementing it on a test network and the simulation results are presented in Section 5. Finally, Section 6 concludes the paper.

2. Overview of the planning model

Fig. 1 shows the general framework of the model presented in this study. As shown in this figure, first, based on the characteristics of the hurricane, the impact of the hurricane on the network components is determined. It is noteworthy that the model presented in this article is based on the work done in [35–37].

The hurricane is characterized by its impacts on the network components when it passes through the network at different speeds. In fact, the wind speed models the intensity of the hurricane, and each part of the network senses a different wind speed, and this wind speed ultimately determines the outages of the network. Respectively, the wind speed at the location of different network components depends on various factors such as the distance of the network components from the eye of the hurricane, the maximum wind speed and the maximum radius of the hurricane. The central point of the hurricane is designated as the eye of hurricane. The farther we go from this point to the points on the circumference of the circle, which is also called the wall of the hurricane eye, the wind speed increases. On the other hand, the further away we are from the wall of the hurricane eye, the wind speed, which is the intensity of the hurricane, decreases.

In order to model the hurricane and determine its impact on the components of the distribution network, two main parameters of the hurricane, (i.e., hurricane intensity-maximum wind speed and hurricane path) will be determined based on the characteristics of the hurricane. It should be noted that all of the characteristics are determined based on historical data, according to which future hurricanes and their impacts on the network can be predicted. In fact, this data will predict the most likely future hurricanes, based on which the distribution network can be planned. According to Fig. 1, the hurricane intensity is determined based on the hurricane eye pressure difference criteria which is the difference between hurricane central pressure and the ambient pressure. Moreover, to determine the path of the hurricane along the time horizon, three other components of the hurricane, i.e., translation velocity, approach angle, and landfall location, are determined. After determining the

Table 1
Taxonomy of research works related to this study.

	Hurricane	Enhancement strategies				Uncertainty	Power section	
		Reliability	Resilience	Automation System	Energy Storage		Distribution system	Transmission system
[11], [13], [18], [14]	-	-	✓	-	-	✓	✓	-
[12]	✓	-	✓	-	-	✓	✓	-
[20], [30], [31]	-	-	✓	-	✓	-	✓	-
[25]	-	-	✓	✓	-	-	✓	-
[26]	-	✓	-	✓	-	-	✓	-
[27]	-	✓	-	✓	-	-	✓	-
[32]	✓	-	✓	✓	-	-	✓	-
[33]	-	-	✓	-	✓	✓	✓	-
This Paper	✓	-	✓	✓	✓	✓	✓	-

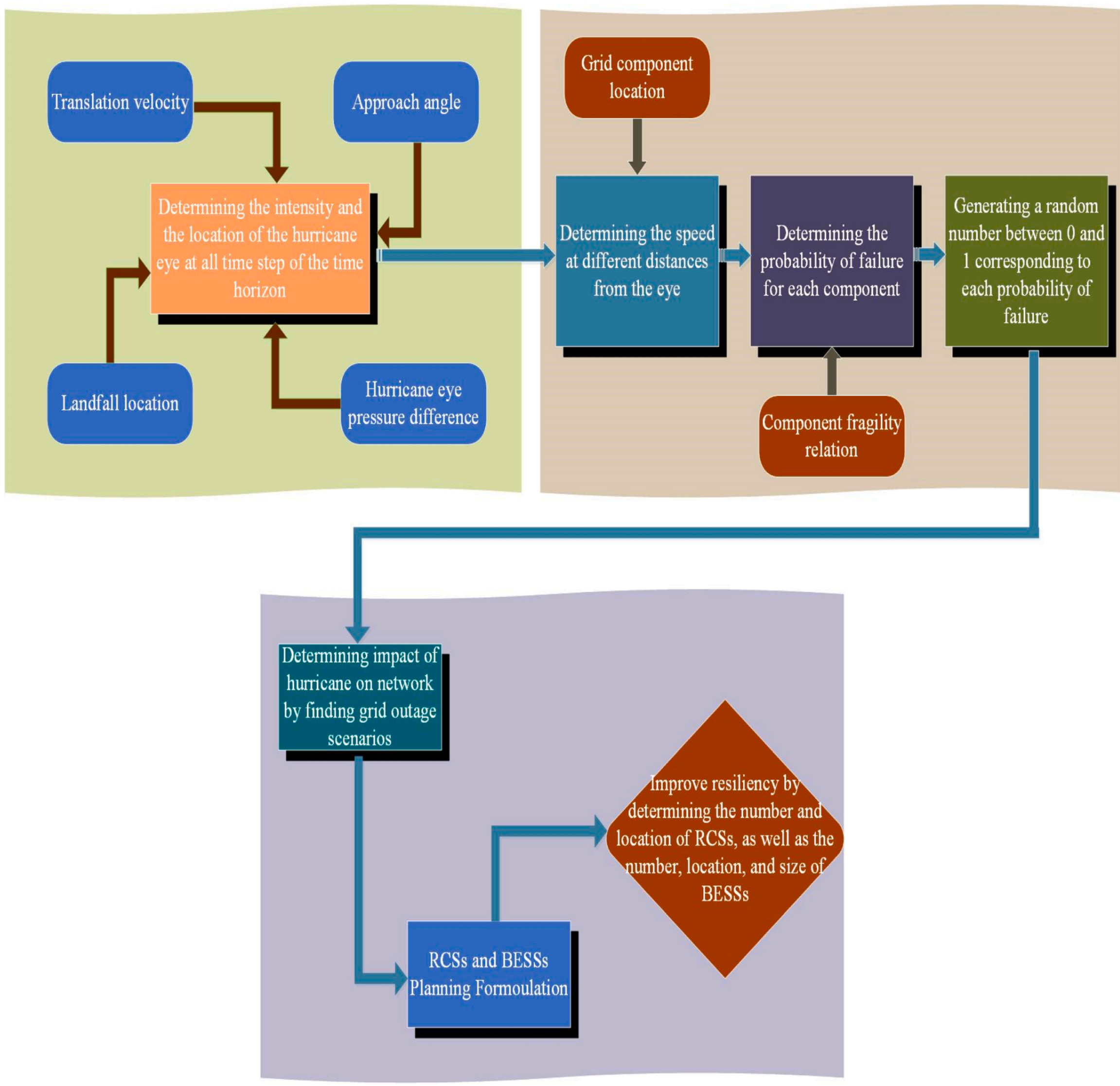

Fig. 1. Proposed planning framework.

characteristics of the hurricane and the position of the eye of the hurricane, the wind speed is determined at different points of the network. Finally, using the equipment failure relationship, network outage scenarios will be determined. Once the impact of future hurricanes on network components is determined, it is entered as input data into the programming formulation to determine the optimal location and number of remote-control switches and the optimal number, location, and size of battery storages to improve the resilience of the distribution network.

3. Hurricane hazard modeling and characterization

To plan a resilient distribution network against hurricanes, one must first predict future hurricanes and determine their impacts on the network. As mentioned in Part 2, to foreseen future hurricanes, hurricane characteristics must be determined based on the historical data. In this part, after determining the characteristics and modeling the hurricane, the scenarios of future hurricanes and the associated network outage scenarios are determined.

3.1. Hurricane intensity and hurricane path

As noted earlier, to determine the intensity of the hurricane, the hurricane eye pressure difference is determined using the following equation [38].

$$p(\Delta P_s) = \frac{k}{C}\left(\frac{\Delta P_s}{C}\right)^{k-1} e^{-\left(\frac{\Delta P_s}{C}\right)^{k}} \tag{1}$$

Eq. 1 shows a Weibull distribution with shape k and scale C parameters. ΔP_s shows the eye pressure difference in each scenario. The Weibull distribution parameters are obtained from historical data. The eye pressure of the hurricane P_s^{eye} is calculated using 2, in which P^{atm} is the average pressure at sea level, which is considered to be approximately equal to 1013 mbar.

$$P_s^{eye} = P^{atm} - \Delta P_s \tag{2}$$

By calculating the hurricane eye pressure, the maximum wind speed can be determined using Table 2, designated as the Saffir-Simpson table.

The path of the hurricane and specifically the position of the eye of the hurricane is determined after determining the three components of the hurricane, i.e., translation velocity, approach angle and landfall location along the time horizon. Translation velocity is the moving speed of the hurricane eye and is determined based on the lognormal distribution and actually represents the time dimension of the movement path. Approach angle and landfall location, which determine the

Table 2
Saffir-Simpson hurricane scale.

Hurricane Category	Central Pressure [mbar]	Wind Speed [m/s]	Damage
1	> 979	33–42	Minimal
2	965–979	43–49	Moderate
3	945–964	50–58	Extensive
4	920–944	58–70	Extreme
5	< 920	> 70	Catastrophic

spatial dimension of the eye movement path, are determined based on the normal distribution [35,39]. In Eqs. 3 to 5, c_s, ϕ_s and Δx_s are respectively translation velocity, approach angle and landfall location. Note that the mean values and standard deviations are determined using the historical data. Fig. 2 shows how to determine the path of hurricane.

$$P(c_s) = \frac{1}{c_s\sqrt{2\pi}\sigma_{ln}}\exp\left[-\frac{1}{2}(\ln(c_s) - \mu_{ln}) \Big/ \sigma_{ln}\right] \tag{3}$$

$$P(\phi_s) = \frac{1}{\sigma_\phi\sqrt{2\pi}}\exp\left[-\frac{1}{2}\left(\frac{\phi_s - \mu_\varnothing}{\sigma_\phi}\right)^2\right] \tag{4}$$

$$P(\Delta x_s) = \frac{1}{\sigma_x\sqrt{2\pi}}\exp\left[-\frac{1}{2}\left(\frac{\Delta x_s - \mu_x}{\sigma_x}\right)^2\right] \tag{5}$$

After determining the characteristics of the hurricane path, the location of the hurricane eye can be determined at each time step of the time horizon [36].

$$Y_{s,t} = c_s t - \frac{Y_s^{tot}}{2} \tag{6}$$

$$Y_s^{tot} = c_s TH \tag{7}$$

Where, $Y_{s,t}$ and Y_s^{tot} show the location of hurricane eye in scenario s at time t as well as the total distance traveled by the hurricane in the time horizon, TH, respectively.

3.2. Wind speed at grid component locations

To determine the speed of the hurricane at different points of the network, first, the wind speed will be determined at any distance from the eye of the hurricane based on the following relationships [35,36,40].

$$ln\ R_s^{max} = 2.556 - 0.000050255\Delta P_s^{\ 2} + 0.042243\psi \tag{8}$$

$$f = 2\Omega \sin\alpha \tag{9}$$

$$B_s = \frac{V^{m2}\rho e}{\Delta P_s} \tag{10}$$

$$A_s = R_s^{maxB_s} \tag{11}$$

$$V_s(r) = \left[\frac{A_s B_s(\Delta P_s)e^{-\frac{A_s}{r^{B_s}}}}{\rho r^{B_s}} + \frac{r^2 f^2}{4}\right]^{1/2} - \frac{rf}{2} \tag{12}$$

Where, R_s^{max} is radius to the maximum wind and ψ is the hurricane latitude. f is Coriolis parameter and Ω is the angular velocity. α is the local latitude. A_s and B_s are shape parameters. V^m is the maximum wind speed determined through Table 2 and P is the density of air, which has a value of 1.225 kg/m^3. Finally, $V_s(r)$ represents the wind speed that the hurricane affects a point at distance r. In order to determine the wind speed at different points of the network, it is necessary to obtain the distance of each point of the network from the eye of the hurricane as follows [36]:

$$x'_{i,s} = (x_i + \Delta x_s)\cos(\phi_s) + y_i \sin(\phi_s) \tag{13}$$

$$y'_{i,s} = -(x_i + \Delta x_s)\sin(\phi_s) + y_i \cos(\phi_s) \tag{14}$$

$$D_{i,t,s} = \sqrt{\left(Y_{s,t} + y'_{i,s}\right)^2 + \left(x'_{i,s}\right)^2} \tag{15}$$

Where, i is an index for network components. Moreover, x_i and y_i show the location of each component of the network relative to the estimated landfall location. Meanwhile, $x'_{i,s}$and$y'_{i,s}$ show the location of each point

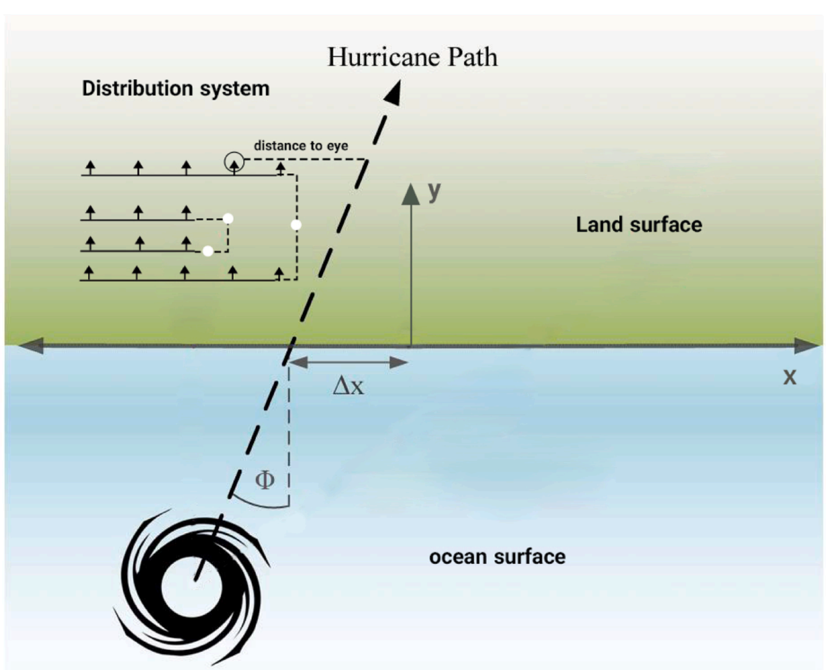

Fig. 2. Spatial-temporal path of the hurricane.

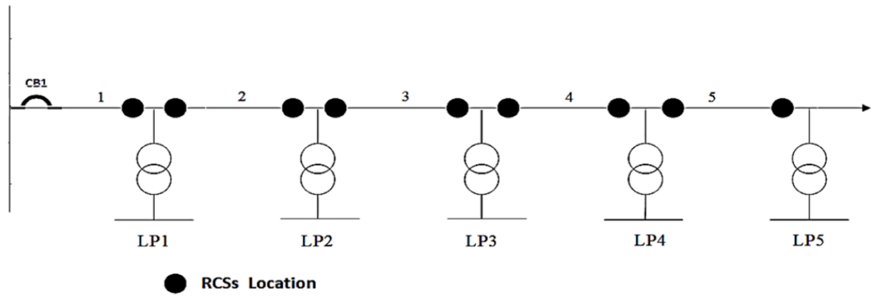

Fig. 3. Network feeder.

of the network after aligning with the hurricane path. Finally, the radial distance of each part of the network to the hurricane eye is determined using (15). $D_{i,t,s}$ represents the radial distance of each component to the eye, which is determined in each scenario and at each time through (15). By replacing the $D_{i,t,s}$ obtained from (15) instead of r in (12), it is possible to determine the wind speed at the location of each component of the network.

3.3. Network outage scenarios

After determining the wind speed at different points of the network, the failure probability of each equipment is obtained using (16), which shows the equipment fragility relationship [41].

$$P_l^f = \alpha I_l (V^r)^\beta \tag{16}$$

In this formulation, I_l is the length of the line in kilometers. P_l^f is the probability of failure, which is known to be determined relative to the hurricane intensity V^r. Actually, V^r is the speed that each component is affected by the hurricane. Also, α and β are fixed values that are equal to 2×10^{-17} and 9.91, respectively. It should be noted that there are two modes of damage and failure for each line during the hurricane passing through the network: 1) the fall of broken trees on the network lines, and 2) the direct breaking of the foundations (poles) by the force of the wind [41], which are considered in (16). After calculating the probability of component failure, a random number between 0 and 1 corresponding to each probability is obtained by generating a uniformly distributed random number. If the probability obtained from (16) is greater than the corresponding random number, it means the failure of the component. As a result, network outage scenarios are determined for each moment of the time horizon. It is noteworthy that if a line fails, it cannot be repaired until the end of the hurricane. Therefore, the line remains failed for the remainder of time horizon.

4. Proposed model for simultaneous planning of distribution automation and energy storage systems

Although the use of various tools such as remote-control switches and energy storage systems improve the state of grid resilience as well as reduce extensive and long outages; these impose costs including investment costs on distribution companies. Therefore, according to this issue, a trade-off should be made between the optimal network resilience level and the costs. In this study, the minimization of investment costs is considered as an objective function. The optimal level of resilience, which is the sum of the interruption costs of customers in the network, is considered as a constraint in the planning problem. The objective function in the mathematical modeling of this problem is as follows:

$$\min \sum_n NESS(n) \times C_{BESS}^f + \left(C_P^{BESS}\, P_{max}^{BESS}(n) + C_E^{BESS}\, E_{max}^{BESS}(n)\right) + \sum_f \sum_h N_{f,h}^{sw} \times C_{sw}^f \tag{17}$$

In this objective function, the first term is related to all investment costs of energy storages. Also, the maximum power cost and the maximum energy cost of each storage device are considered. In fact, this maximum power/energy determines the storage capacity. The last term represents the investment cost for RCSs and the goal of optimization is to minimize the overall costs.

In this study, a stochastic mixed integer linear programming (MILP) with the following constraints is formulated for simultaneous planning of distribution automation and energy storage systems.

4.1. Power flow constraints

In this study, the DC power flow model developed in [42,43] is applied for modeling the network operation. Respectively, the constraints of this optimization problem are as follows:

$$P_n^D - \sum_u P_{u,s,t}^G - P_{n,s,t}^{LC} - P_{n,s,t}^{BESS} + \sum_f \sum_l Pf_{f,l,s,t}^s AC_{f,l,n} + \sum_f \sum_l Pf_{f,l,s,t}^r BC_{f,l,n} = 0, \quad \forall n,s,t \tag{18}$$

$$Pf_{f,l,s,t}^s \le b_{f,l}\Big(\sum_n \delta_{n,s,t} AC_{f,l,n} - \sum_n \delta_{n,s,t} BC_{f,l,n}\Big) + \vartheta_{f,l,s,t} M, \quad \forall f,l,s,t \tag{19}$$

$$Pf_{f,l,s,t}^s \ge b_{f,l}\Big(\sum_n \delta_{n,s,t} AC_{f,l,n} - \sum_n \delta_{n,s,t} BC_{f,l,n}\Big) - \vartheta_{f,l,s,t} M, \quad \forall f,l,s,t \tag{20}$$

$$Pf_{f,l,s,t}^r \le b_{f,l}\Big(\sum_n \delta_{n,s,t} BC_{f,l,n} - \sum_n \delta_{n,s,t} AC_{f,l,n}\Big) + \vartheta_{f,l,s,t} M, \quad \forall f,l,s,t \tag{21}$$

$$Pf_{f,l,s,t}^r \ge b_{f,l}\Big(\sum_n \delta_{n,s,t} BC_{f,l,n} - \sum_n \delta_{n,s,t} AC_{f,l,n}\Big) - \vartheta_{f,l,s,t} M, \quad \forall f,l,s,t \tag{22}$$

$$Pf_{f,l,s,t}^s \le cap_{f,l}\big(1 - \vartheta_{f,l,s,t}\big), \quad \forall f,l,s,t \tag{23}$$

$$Pf_{f,l,s,t}^s \ge -cap_{f,l}\big(1 - \vartheta_{f,l,s,t}\big), \quad \forall f,l,s,t \tag{24}$$

$$Pf_{f,l,s,t}^r \le cap_{f,l}\big(1 - \vartheta_{f,l,s,t}\big), \quad \forall f,l,s,t \tag{25}$$

$$Pf_{f,l,s,t}^r \ge -cap_{f,l}\big(1 - \vartheta_{f,l,s,t}\big), \quad \forall f,l,s,t \tag{26}$$

$$P_{u,s,t}^G \le cap_u^G, \quad \forall n,s,t \tag{27}$$

$$P_{n,s,t}^{LC} \le P_n^D, \quad \forall n,s,t \tag{28}$$

$$P_{u,s,t}^G \le P_u^{G,max}, \quad \forall u \tag{29}$$

$$\delta_{n,s,t} \le \frac{\pi}{6}, \quad \forall n,s,t \tag{30}$$

$$\delta_{n,s,t} \ge -\frac{\pi}{6}, \quad \forall n,s,t \tag{31}$$

Eq. (18) shows active power balance at each bus, in each scenario and at each time step. In fact, the loads placed at each bus are either supplied by the main network, or supplied by energy storage, or they have to be curtailed. Constraints (19) - (22) determine the power exchange at each bus based on the bus voltages. As can be seen, in these relations, the big-M method has been used to ensure that voltage angles of the two buses holding a line are independent if the line is in an open status. It should be noted that in these relationships, if line (l) is connected to bus n from upstream, $AC_{f,l,n}$ takes the value of one. Otherwise, this variable does not take any value, which means that bus n is not connected to line (l). Also, if line (l) is connected to bus n from downstream, $BC_{f,l,n}$ will take the value of one and otherwise it will not take any value. Constraints (23) - (26) show that flowing power through a line depends on both line status and line capacity. It means that if a line is not faulted and the line is in a healthy state, the power passing through this line is within the capacity of the line, and if the line is faulted or is not isolated from another fault in the network, no power can pass through the line. Constraint (27) limits the output power of generators and constraint (28) shows the maximum amount of power that could be curtailed in each bus compared to the total load of the bus. Constraint (29) puts limitation over the generated and transmitted power from upstream. Constraints (30) and (31) also limit the voltage angles to a specific value.

4.2. Energy storages optimization constraints

The constraints related to determining the size, number and location of storages are as follows:

$$SOC_{n,s,t} = (1-\partial) * SOC_{n,s,t-1} - \frac{P^{BESS}_{n,s,t}\Delta t}{\eta_d}, \quad \forall n,s,t \tag{32}$$

$$SOC_{n,s,t} \le NESS(n)\ .\ SOC^{max}_n, \quad \forall n,s,t \tag{33}$$

$$P^{BESS}_{n,s,t}(n) \le P^{BESS}_{max}(n), \quad \forall n,s,t \tag{34}$$

$$P^{BESS}_{max} \le \sum_n P^D_n, \quad \forall n \tag{35}$$

$$E^{BESS}_{max}(n) \ge P^{BESS}_{max}(n)\ .\ TH, \quad \forall n,s,t \tag{36}$$

Eq. (32) specifies the charging status of the storages over time. In this regard, only the storage discharge mode is considered and its charging mode is ignored. The reason for this is that during extreme events, part of the network is separated from the main network, and naturally, the parts of the network that are connected to the main network are still supplied and there is no need for storages. However, the formulation could be easily expanded to consider the charging status of the storages. In fact, it is possible to charge the storages when they are connected to the network. It should also be noted that many events, including hurricanes, are predictable. According to [44], it is possible to predict a hurricane from 24 to 72 hours in advance. Therefore, the storage units can be charged before the start of the hurricane, and thus they can supply the disconnected loads after the occurrence. Constraint (33) indicates state-of-charge (SOC) limit. The output power of the storage in each scenario and at any time can have a value equal to the maximum power capacity of the storage and also the maximum output power of the storage is limited to the sum of the loads in the network which are shown in (34) and (35), respectively. Also, constraint (36) considers the minimum storage energy capacity equals to the product of the maximum storage power capacity in the planning time horizon. In fact, this constraint considers the maximum possible amount associated with the discharge of storage units and it ensures that the storage capacity is sufficient to supply the load in the planning time horizon. In general, in this method, an initial value SOC^{max}_n is considered as the energy capacity of the storage, and finally the maximum amount of discharge in each storage is considered as the energy capacity of that storage.

$$E^{BESS}_{max}(n) \ge SOC_{n,s,t}, \quad \forall n,s,t \tag{37}$$

If (37) is used instead of (36), the storage capacity is not determined according to the demand value, and a fixed value for the capacity is considered for all storage units. Naturally, in the first method, the best condition is obtained for the storage capacity and there would be no energy loss. This issue is discussed in the numerical results section.

4.3. Remote control switches optimization constraints

During extreme events, several lines may fail in each feeder network. Depending on the location of the switches and the position of the faulted sections in the network feeder, it is possible to determine whether power flow can be obtained for each line. If there is a fault in a line, it is clear that no power flow can be taken for that line and $\vartheta_{f,l,s,t}$ will be equal to one. But the lines without fault can be divided into three main groups according to the fault positions on distribution feeder. The first group of lines (GL1) is those located between the higher voltage substation and the first faulted section on distribution feeders. These lines can be re-energized if a switch is placed between these lines and the first faulted section. The second group of lines (GL2) is those located between two faulted sections in the network feeder. These lines can be re-energized if they are isolated from both faults. The third group of lines (GL3) is those located downstream of the last faulted section on distribution feeder and these lines are re-energized if any switch is located between them and the upstream fault. For example, the following feeder is considered.

If a fault happens in line 2 and line 4, lines 1, 3, and 5 which have no faults, will be in GL1, GL2, and GL3, respectively. If a line has not failed, then the condition of the line can be considered healthy and the power flow can be taken for that line after isolating the faulted lines. The isolation is done by the switches placed on both sides of the line. According to the number of faulted sections in each distribution feeder, the following equations will determine the status of each line.

$$\vartheta_{f,l,s,t} = 0, \quad \forall f,l,s,t,d^1_{f,s,t} \in \varnothing \tag{38}$$

$$\vartheta_{f,l,s,t} = 1, \quad \forall f,l,s,t,l = d^1_{f,s,t} \tag{39}$$

$$\vartheta_{f,l,s,t} = 1 - \sum_{h=2l}^{2d^1_{f,s,t}} N^{sw}_{f,h}, \quad \forall f,l,s,t,l < d^1_{f,s,t} \tag{40}$$

$$\vartheta_{f,l,s,t} = 1 - \sum_{h=2d^1_{f,s,t}-1}^{2l-1} N^{sw}_{f,h}, \quad \forall f,l,s,t,l > d^1_{f,s,t} \tag{41}$$

$$\vartheta_{f,l,s,t} = 1, \quad \forall f,l,s,t,l = d^1_{f,s,t} \tag{42}$$

$$\vartheta_{f,l,s,t} = 1, \quad \forall f,l,s,t,l = d^2_{f,s,t} \tag{43}$$

$$\vartheta_{f,l,s,t} = 1 - \sum_{h=2l}^{2d^1_{f,s,t}} N^{sw}_{f,h}, \quad \forall f,l,s,t,l < d^1_{f,s,t} \tag{44}$$

$$\vartheta_{f,l,s,t} = 1 - \sum_{h=2d^2_{f,s,t}-1}^{2l-1} N^{sw}_{f,h}, \quad \forall f,l,s,t,l > d^2_{f,s,t} \tag{45}$$

$$\vartheta^1_{f,l,s,t} \ge 1 - \sum_{h=2d^2_{f,s,t}-1}^{2l-1} N^{sw}_{f,h}, \quad \forall f,l,s,t,l > d^1_{f,s,t} \tag{46}$$

$$\vartheta^2_{f,l,s,t} \ge 1 - \sum_{h=2l}^{2d^2_{f,s,t}} N^{sw}_{f,h}, \quad \forall f,l,s,t,l < d^2_{f,s,t} \tag{47}$$

$$\vartheta_{f,l,s,t} \ge \vartheta^1_{f,l,s,t}, \quad \forall f,l,s,t,d^1_{f,s,t} < l < d^2_{f,s,t} \tag{48}$$

$$\vartheta_{f,l,s,t} \geq \vartheta^2_{f,l,s,t}, \quad \forall f, l, s, t, d^1_{f,s,t} < l < d^2_{f,s,t} \tag{49}$$

$$\vartheta_{f,l,s,t} \leq \vartheta^1_{f,l,s,t} + \vartheta^2_{f,l,s,t}, \forall f, l, s, t, d^1_{f,s,t} < l < d^2_{f,s,t} \tag{50}$$

Eq. (38) shows that the status of the lines that are in a feeder without fault is equal to zero. In these relations and according to power flow constraints, the number zero means that the line is healthy and while 1 indicates a failure in the line or the line is not isolated from a fault in the network. Constraints (39) - (42) are presented for the feeders with only one faulted section. Eq. (39) sets the status of the faulted line equal to one. Eq. (40) is for the lines that are located between the higher voltage substation and the faulted section on distribution feeder. It examines whether there is any switch between the faulted section and its upstream line (l). In the case of existing at least one switch, line (l) is isolated from the faulted section and $\vartheta_{f,l,s,t} = 0$, otherwise, it is not isolated and $\vartheta_{f,l,s,t} = 1$. The relation (41) is for the lines that are located downstream of the faulted section and examines whether there is any switch between the faulted section and its downstream line (l). If there is at least one switch, line (l) is isolated from the faulted section and $\vartheta_{f,l,s,t} = 0$, otherwise, it is not isolated and $\vartheta_{f,l,s,t} = 1$. Constraints (42) - (50) are provided for feeders with two simultaneous faults. Similar to (38), Eqs. (42) and (43) specify the status of faulted sections of distribution feeder. These equations set the status of the first and second fault sections of feeder equal to 1, respectively. Eq. (44) specifies the state of the lines upstream of the first fault section and examines whether there is any switch between the first faulted section and its upstream line (l). If there is at least one switch, line (l) is isolated from the faulted section and $\vartheta_{f,l,s,t} = 0$, otherwise, it is not isolated and $\vartheta_{f,l,s,t} = 1$. Eq. (45) does the same for the lines downstream of the second fault section. In the case of simultaneous outage of two sections from the feeder, in addition to determining the status of the lines upstream of the first fault section and downstream of the second fault section, the status of the lines between two fault sections must also be determined. In order to be able to take power flow for the lines that are placed between two fault sections, these lines must be isolated from both faults at the same time. Constraints (46) and (47) check the status of the lines between two fault sections relative to the upstream (i.e., the first fault section) and relative to the downstream (i.e., the second fault section) according to the position of the switches, respectively. To determine the final condition of the lines, the result of these two constraints must be considered together to check the simultaneous isolation from upstream and downstream networks. To ensure adherence to the linearity of the problem, relations (48–50) added to check the simultaneous isolation from upstream and downstream networks. These relations confirm that power flow can be obtained for the lines between two fault sections only if the switches separate these lines from both faults. In the same way, it can be written relationships for feeders with three simultaneous faults. Considering extreme events such as hurricanes may cause all the lines of a feeder to fault. So, these relationships should be written for feeders with simultaneous outage of all lines. In this study, according to the test system of Section 5, these relationships should be written for feeders with simultaneous outage of 5 lines.

4.4. Resilience level constraints

As mentioned, in this study, the level of resilience is considered as follows:

$$\sum_n \sum_s \sum_t pr(s) P^{LC}_{n,s,t} CDF^{RE}_{n,t} \leq cdf^{total} \tag{51}$$

Constraint (51) states that the total cost of the interrupted load in all scenarios and times is less than a certain value. This indicates that if this value is equal to zero, all network loads are supplied, which implies the 100 % resilience in the article. In this study, different levels are considered and checked for resilience. Nevertheless, as a base case, cdf^{total} is considered equal to half of the total costs of interrupted load in all scenarios and times. In fact, this relationship shows that in the base case, planning will be done in such a way that the resilience level in the network is improved by 50 %.

4.5. Technical and economic constraints

In this section, some other constraints that are used in this planning problem are presented in order to check their impacts on the cost and level of resilience.

$$\sum_n NESS(n) \leq N^{BESS}_{\max} \tag{52}$$

$$\sum_f \sum_h N^{sw}_{f,h} \leq N^{sw}_{max} \tag{53}$$

$$\sum_n NESS(n) \times C^f_{BESS} + \left(C^{BESS}_P P^{BESS}_{max}(n) + C^{BESS}_E E^{BESS}_{max}(n)\right) + \sum_f \sum_h N^{sw}_{f,h} \times C^f_{sw} \leq Budget \tag{54}$$

Eq. (52) limits the number of network storages to a certain value, and (53) limits the number of RCSs in the network. Eq. (54) includes budget constraints in the planning problem. It should be noted that due to the fact that the most optimal cost at a specific resilience level is obtained from solving the optimization problem, then limiting the budget to an amount lower than the obtained cost will cause the problem to have no solution, which will be investigated in the numerical results.

Considering the objective function (17) and related constraints (18–54), the simultaneous planning of RCSs and BESSs is formulated in the form of MILP, which can effectively be solved by available solvers. The main input data of the optimization model includes equipment cost data, including the installation and investment costs of RCSs and BESSs, the set of candidate locations for equipment installation, network configuration in each scenario, desired resilience level, as well as technical and economic limitations. The decision variables are the location of RCSs and BESSs along with storages capacity. Finally, the output data is the number and location of switches as well as the number, location and size of storages according to the desired level of resiliency in the network as well as system costs.

5. Numerical results

In this section, to evaluate the efficiency of the proposed model, it is implemented on Bus 4 of the Roy Billinton Test System (RBTS) shown in Fig. 4. The test system information was taken from [45]. The model is solved using CPLEX v12.8.0.0 on GAMS v26.1.0. For the input parameters presented in this case study and a MILP optimality gap of 0.0 %, the solver finds a solution to the model in 24.11 seconds on a 2.50 GHz processor and 32 GB RAM.

As shown in Fig. 4, this test system is placed in a two-dimensional coordinate, which indicates the position of the grid components. In the lines of this network, the poles are placed next to each other according to the existing standards, with a distance of 100 m. The length of each line is assumed to be 5 km. This network includes 38 load points located in 29 buses. There are three types of loads in this network, and the customer damage function for all types of loads is shown in Table 3.

With a slight difference compared to the information given in [44], all the loads in Buses 5, 13, 18 and 29 are considered to be commercial. Actually, they are considered as critical loads. As a result, using Table 3, the priority of critical loads is considered.

To predict future hurricanes and check their impacts on the network components according to what was explained in Sections 2 and 3, 300 scenarios for each of the characteristics of the hurricane (i.e., hurricane

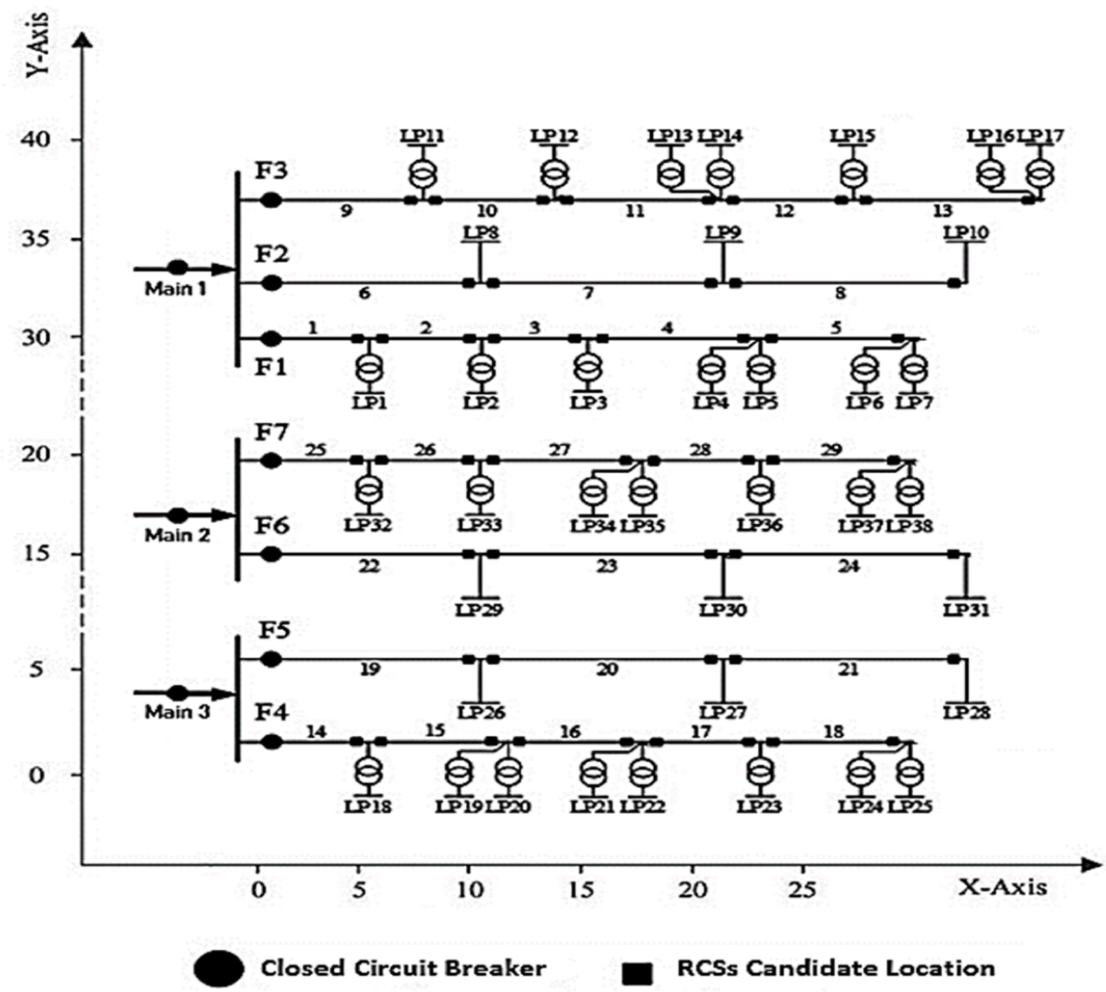

Fig. 4. Roy Billinton Test System bus number 4 (distances are in km).

Table 3
Customer damage function.

Customer type	Interruption cost in different duration [k$/MW]			
	1 min	5 min	60 min	600 min
Residential	0.011	0.055	0.667	6.67
Industrial	0.064	0.321	3.85	38.5
Commercial	0.072	0.362	4.35	43.5

intensity, approach angle, landfall location and translation velocity) is produced based on historical data. This data was extracted based on the historical data recorded from 64 hurricanes occurred in a region in USA between 1850 and 2008 [35]. Mean values (m) and standard deviations (σ) for each hurricane characteristic based on historical data are given in Table 4 [35]. After generating scenarios for each characteristic, the

Table 4
Region-specific parameter.

Hurricane Characteristics	Parameter	Value
Eye Pressure Difference	C	33
	K	1.4
Approach angle	M	−27.63
	σ	44.13
Landfall location	M	0
	σ	5
Translation velocity	M	3.1
	σ	0.35

number of scenarios is reduced to 10 scenarios using the k-means algorithm. Finally, each of the obtained scenarios for characteristics constitute a hurricane scenario, respectively. Then, we pass each of the hurricane scenario through the test system for 24 hours to obtain the outage scenarios of the network components at each time-step. These scenarios show the status of each line in each scenario and at any time. These data, which actually show the configuration of the network, are used as input data to the model provided for optimization planning.

After predicting the impact of future hurricanes on distribution network components, the presented model for simultaneous planning of distribution automation and energy storage systems is implemented on a test system to check the effectiveness of the proposed model. The cost of each remote-control switch is considered to be 4700 dollars [46]. The candidate locations for installing switches are assumed to be the first and last point of each line. So according to Fig. 5, in each feeder with five lines, there are 9 candidate places for installing switches.

In this research, the battery energy storages are assumed to be lithium-ion type. Therefore, the fixed cost C^{f}_{BESS} for each storage is assumed to be equal to 1 M$, and the variable costs including power costs C^{BESS}_{P} and energy C^{BESS}_{E} are 175,000 $/MW and 500,000 $/MWh, respectively [33,47]. Also, the discharge efficiency for energy storage is assumed to be 0.95. Each bus of the network can be a place to install the storage, which is finally determined in the planning. The capacity of each generator and the capacity of each line are considered to be equal to 30 and 10 MW, respectively. In fact, it is assumed that there is no shortage in the field of generation and transmission. Also, SOC^{max}_{n} which is given to the program as an initial value for the size of the storages, is

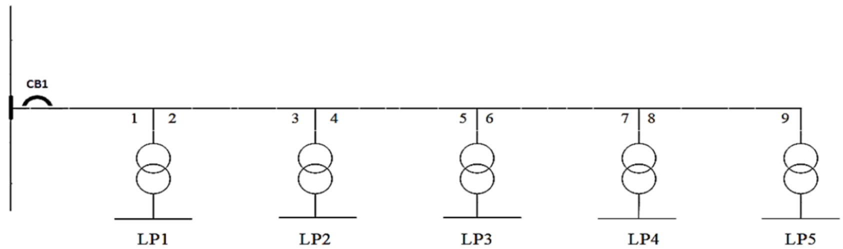

Fig. 5. Candidate node for RCSs location.

assumed to be large enough.

5.1. Planning without technical and economic constraints

First, the two study methods presented in Section 4 have been numerically compared to determine which method is more optimal. In the first method, the capacity of energy storage is determined according to the need in each bus. While in the second method, a fixed capacity equal to 50 MW/h is considered for each battery storage installed in the network. The numerical results for these two methods are given in Table 5.

As the numerical results reveal, the first method shows the most optimal state. Because a lower storage capacity may be needed in a bus than the fixed assumed capacity. In the optimal method, the cost is lower, because the amount of energy storage capacity installed in the network is lower. The output power of the storage is slightly higher in the second method, which increases the supplied power for that part of the network where the storage is installed. As a result, fewer switches are needed to improve resilience. It should be noted that in both methods the base case, which is reaching the 50 % resilience level, is considered as the goal.

The diagram in Fig. 6 shows how the cost changes to reach different levels of resilience.

As it is clear from this diagram, in order to reach the resilience level of 100 % (i.e., when no load is interrupted), a lot of cost is imposed on the distribution company. As the cost has significantly increased from 60 % to 100 % resilience level, it seems that resilience levels between 50 % and 60 % could be considered the levels of resilience that can be justified for investing in the network.

The diagram in Fig. 7 shows that distribution automation alone can make the network resilient to some extent. However, in order to reach higher levels of resilience, along with distribution automation, energy storages should be used in the network planning. In fact, at lower resilience levels, placement of switches has improved resilience and placement of storages has led to higher resilience levels. The number of switches in medium resilience levels is almost constant, which somehow shows that the use of distribution automation improves resilience up to a certain level, and for higher levels, other strategies to improve resilience should be taken into account. The reason for this is that in an extreme event, all the lines of a feeder may have failed. In this situation, fault isolation alone cannot restore the loads in that feeder. Therefore, even though the cost of using distribution automation is much lower than using storages in the network, it is necessary to use storages in these cases to supply loads, especially critical loads. Also, as it is clear from Fig. 7, in order to reach 100 % resilience, a storage must be used in most

Table 5
Comparison of two study methods.

Methods	Cost ($)	RCS number	BESS number	E_{max}^{BESS} (MWh)	P_{max}^{BESS} (MW)
Optimal Capacity	20,463,569.76	7	1	38.46	1.13
Fixed Capacity	25,573,653.16	2	1	50	1.34

of the network buses, which explains the reason for the high cost to reach this level.

Another point that can be obtained from Fig. 6 and Fig. 7 is that although the number of switches and storages are the same at 40 % and 50 % resilience levels, the cost is different. The reason for this is that despite the fixed number of switches and storages installed in the network, the amount of capacity and energy of the storages installed in the network is different. In fact, to change the resilience level from 40 % to 50 %, there is no need to install a new key or a storage unit, but it is enough to increase the power and energy of the installed storages in the network. Fig. 8 shows the variations in the maximum power and capacity of the storage units installed on bus 13 in 3 scenarios where the number of storages and switches remains constant.

This point is clear from Table 6. This table shows the number and location of switches and storage units installed in the network at different resilience levels.

According to Table 6, almost in most levels of resilience, including in the basic state, bus 13 has been a point for installing a storage device in order to improve resilience. One of the reasons for this issue is the importance of the load points of this bus due to their criticality. Moreover, in most of the predicted hurricanes and grid outage scenarios, these load points are isolated from the main network. Also, installing a switch for this point of the network alone cannot provide the critical load on this bus. As a result, this point is one of the weak points of the network, where it is necessary to install storages in order to supply its critical loads. So, it should be mentioned that one of the advantages of the presented model for the simultaneous planning of distribution automation and energy storage is to determine the weak points of the network. Weak points mean the most vulnerable points of the network that are isolated from the network in most hurricane scenarios. By determining these points, maneuvers, and plans can be made for these points to improve the state of resilience in the network. For example, a group can be placed in that place in advance to repair these points as quickly as possible, or these points can be prioritized for repair in order to reduce the required storage capacities in these points and as a result reducing the overall cost.

It can also be seen from Table 6 that in most resilience levels, the location of switches is fixed or changing slightly. Also, in most cases, the switches are installed at the beginning of the feeder section, however, in some resilience levels, it is observed that the switch is installed at the end of the feeder section. The importance of installing the switch at the end of the lines is determined by the fact that, for example, if at the resilience level of 80 %, a switch was not installed at the end of the first grid line from the second feeder, a storage would have to be placed to recover the load in the first bus, which would increase the cost. The importance of supplying critical loads can be seen from the installation of energy storages in the places where critical loads are located (see Table 6). For example, at the resilience level of 70 %, a storage has been placed in most of the buses where the critical loads are located, and almost all the critical loads at this level of resilience have been recovered. In fact, according to Table 6, in most cases, BESSs are installed in buses with critical load points or at the end of the feeder which shows the importance of these points.

Fig. 9 shows the discharge status of the installed energy storage in the

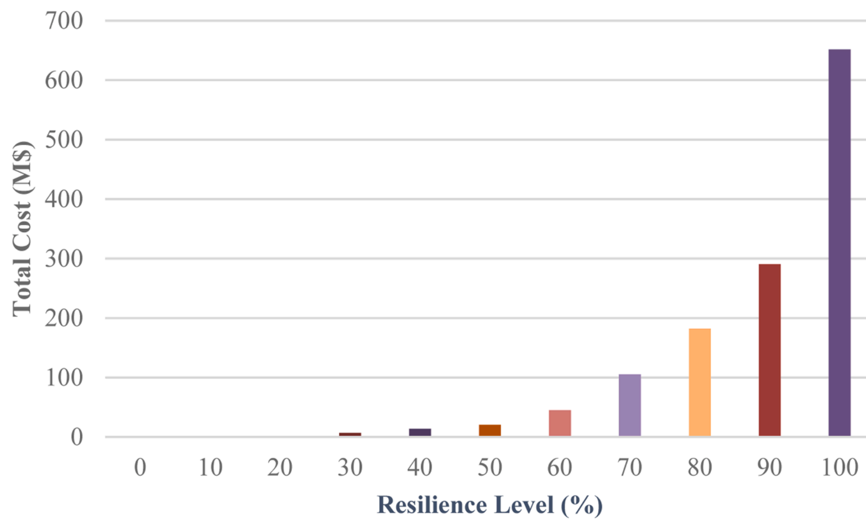

Fig. 6. Cost at different resilience level.

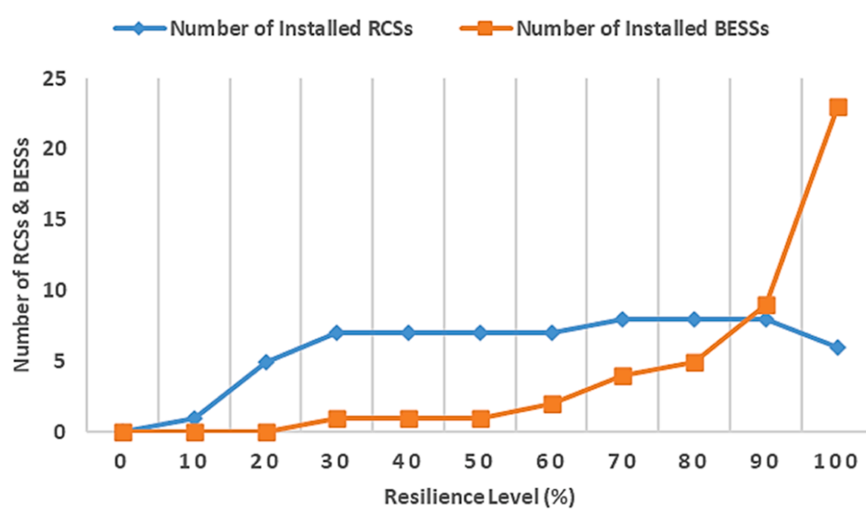

Fig. 7. Number of RCSs and BESSs installed at different resilience level.

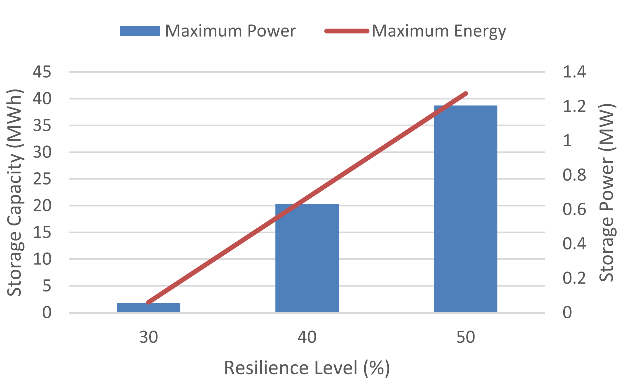

Fig. 8. Storage power and capacity Level for bus 13 at different resilience level.

basic state.

Fig. 9 shows that in one of the predicted scenarios for future hurricanes, from the very first hour of the beginning of hurricane, bus 13 is disconnected from the main network. As a result, the critical load in bus 13 is supplied by the storage unit installed in the grid as shown in Fig. 9.

Table 6
Optimal location of RCSs and BESSs in different resilience levels.

Resilience level	RCSs location (Feeder number, Candidate location (h))	BESSs location (Bus number)
0	-	-
10	3.h8	-
20	1.h8, 2.h4, 3.h8, 5.h2, 6.h2	-
30	1.h8, 2.h4, 3.h8, 4.h4, 5.h2, 6.h2, 7.h8	13
40	1.h8, 2.h4, 3.h8, 4.h4, 5.h2, 6.h2, 7.h8	13
50	1.h8, 2.h4, 3.h8, 4.h4, 5.h2, 6.h2, 7.h8	13
60	1.h8, 2.h4, 3.h8, 4.h4, 5.h2, 6.h2, 7.h8	5. 13
70	1.h8, 2.h1, 2.h4, 3.h8, 4.h4, 5.h2, 6.h2, 7.h8	5, 8, 13, 29
80	1.h8, 2.h1, 2.h4, 3.h6, 4.h4, 5.h2, 6.h2, 7.h8	5, 8, 12, 13, 29
90	1.h8, 2.h1, 2.h4, 3.h6, 4.h4, 5.h2, 6.h2, 7.h8	5, 8, 12, 13, 18, 20, 23, 24, 29
100	1.h2, 2.h1, 2.h4, 3.h2, 4.h7, 5.h2	In all buses except 1, 6, 7, 9, 17, 19

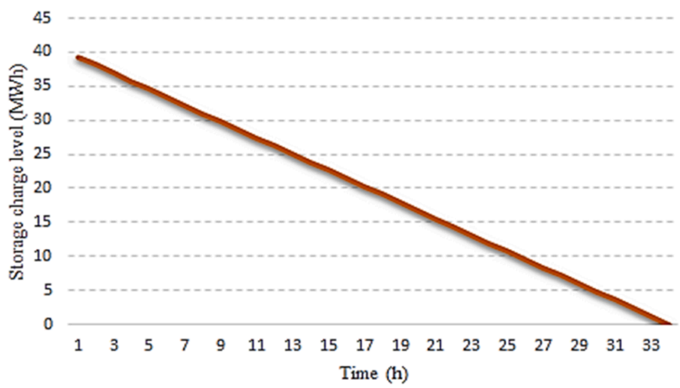

Fig. 9. Storage charge level for bus 13.

5.2. Planning despite technical and economic constraints

Until now, it was assumed that there is no limit to the number of switches installed in the network. Now, in this section, if we limit the number of switches installed in the network, the cost and planning results would be changed in the basic state. Table 7 shows that by limiting the number of switches to be installed in the network, the cost increases. The reason for this is that when the number of switches is limited, it is necessary to increase the capacity of the storage power and energy or the number of storages in order to reach the desired resilience level. It is clear from the table that at first the presented model has tried to reach the optimal level of resilience by increasing the power capacity/energy of storages, but with more restrictions on the number of switches, this model has been forced to install more energy storage in the network. This has resulted in increasing the planning costs.

If there is a limit on the number of energy storages, it is predicted that the program will not be able to meet the optimal conditions for resilience. In fact, as mentioned in the previous sections, distribution automation can partially meet the desired levels of resilience. Despite the lower cost of planning distribution automation in the network, for higher levels of resilience, this solution alone cannot meet the desired conditions. To confirm this, the number of storage devices installed in the network was limited to zero in the base case. On the base case and in the conditions where there was no limitation on the number of storages, one storage with 7 switches would satisfy the conditions of the problem. But with the limitation of storages from one to zero, the optimization problem no longer finds an answer. Because the required conditions for resilience could not be met.

The presented model for this planning presents the most optimal mode (lowest cost) as the answer to the problem. Naturally, if a constraint is imposed on the network budget below the optimal cost obtained in the base case, the problem will no longer have an answer.

6. Conclusions

The implementation of distribution automation in electricity distribution networks provides the possibility of doing tasks faster and also isolating faulted components without human intervention in extreme weather conditions when it is not possible to send a repair team. While, using this method to improve resiliency is less expensive than other solutions such as using energy storages; this study shows that distribution automation can improve resiliency in the network to some extent. Therefore, to reach higher levels of resilience, other solutions such as integrating BESSs should be used along with optimizing the distribution automation system. In this article, a model for simultaneous planning of distribution automation and battery energy storage systems is presented and implemented on a sample network to check its efficiency. The presented model determines the number and location of RCSs as well as the number, location and capacity of BESSs. This model, while showing the importance of supplying critical loads to improve the resilience of the network, can also identify the weak points of the network, which can be used for further planning for these points. Another result of this planning was the increase in cost after restrictions were placed on the use of switches, which shows the importance of simultaneous planning of resilience improvement solutions. As a result, for future work, it is possible to point to the simultaneous planning of other solutions such as grid hardening as well as demand response to improve resilience, which will reduce costs and improve resilience in a cost-effective manner.

Table 7
Planning with a limit on the number of RCSs.

Limitation on the number of RCSs	Cost ($)	RCSs number	BESSs number
Unlimited	20,463,569.76	7	1
5	21,355,674.51	5	1
3	22,772,370.75	3	1
1	33,321,843.76	1	2

CRediT authorship contribution statement

Sadeghian-Jahromi Mohammad: Writing – original draft, Software, Methodology, Conceptualization. **Lehtonen Matti:** Writing – review & editing, Supervision. **Wang Fei:** Writing – review & editing, Supervision. **Fattaheian-Dehkordi Sajjad:** Writing – review & editing, Methodology, Conceptualization. **Fotuhi Firuzabad Mahmud:** Writing – review & editing, Supervision.

Declaration of Competing Interest

The authors declare that they have no known competing financial interests or personal relationships that could have appeared to influence the work reported in this paper.

Acknowledgements

M. Fotuhi-Firuzabad appreciates the Insf for the support of his work.

Data availability

Data will be made available on request.

References

[1] R. Ghorani, S. Fattaheian-Dehkordi, M. Farrokhi, M. Fotuhi-Firuzabad, M. Lehtonen. Modeling and Quantification of Power System Resilience to Natural Hazards: A Case of Landslide 9, IEEE Access, 2021, pp. 80300–80309, https://doi.org/10.1109/ACCESS.2021.3084368.
[2] C. Nicolas et al., Stronger Power, 2019.
[3] E.H. Allen, R.B. Stuart, T.E. Wiedman, No light in August: power system restoration following the 2003 North American blackout, IEEE Power Energy Mag. 12 (1) (2013) 24–33.
[4] J. Najafi, A. Peiravi, J.M. Guerrero, Power distribution system improvement planning under hurricanes based on a new resilience index, Sustain. Cities Soc. 39 (2018) 592–604.
[5] Willie Drye, hurricane season was the most expensive in US history, Natl. Geogr. 30 (2017).
[6] Hines, Paul, Jay Apt, and Sarosh Talukdar. Trends in the history of large blackouts in the United States, in: Proceedings of the IEEE Power and Energy Society General Meeting-Conversion and Delivery of Electrical Energy in the 21st Century, IEEE, 1-8, 2008.
[7] Y. Zhang, N. Yang, U. Lall, Modeling and simulation of the vulnerability of interdependent power-water infrastructure networks to cascading failures, J. Syst. Sci. Syst. Eng. 25 (1) (2016) 102–118.
[8] M. McGranaghan, M. Olearczyk, C. Gellings, Enhancing distribution resiliency: opportunities for applying innovative technologies, Electr. Today 28 (1) (2013) 46–48.
[9] S.A. Fenrick, L. Getachew, Cost and reliability comparisons of underground and overhead power lines, Util. Policy 20 (1) (2012) 31–37.
[10] J. Boggess, G. Becker, M. Mitchell, Storm & flood hardening of electrical substations. in: Proceedings of the 2014 IEEE PES T&D Conference and Exposition, IEEE, 2014, pp. 1–5.

[11] X. Wang, Z. Li, M. Shahidehpour, C. Jiang, Robust line hardening strategies for improving the resilience of distribution systems with variable renewable resources, IEEE Trans. Sustain. Energy 10 (1) (Jan. 2019) 386–395.
[12] M. Ghasemi, A. Kazemi, M.A. Gilani, M. Shafie-Khah, A stochastic planning model for improving resilience of distribution system considering master-slave distributed generators and network reconfiguration, IEEE Access 9 (2021) 78859–78872.
[13] B. Taheri, A. Safdarian, Tie-line planning for resilience enhancement in unbalanced distribution networks, IET Gener. Transm. Distrib. 16 (5) (2022) 1030–1046.
[14] M. Borghei, M. Ghassemi, Optimal planning of microgrids for resilient distribution networks, Int. J. Electr. Power Energy Syst. 128 (2021) 106682.
[15] H.K. Rad, Z. Moravej, An approach for simultaneous distribution, sub-transmission, and transmission networks expansion planning, Int. J. Electr. Power Energy Syst. 91 (2017) 166–182.
[16] J. Salehi, F. Gazijahani, A. Safari, Stochastic simultaneous planning of interruptible loads, renewable‪ generations and capacitors in distribution network‪, J. Oper. Autom. Power Eng. 10 (2) (2022) 113–121.
[17] H. Teimourzadeh, B. Mohammadi-Ivatloo, "A three-dimensional group search optimization approach for simultaneous planning of distributed generation units and distribution network reconfiguration, Appl. Soft Comput. 88 (2020) 106012.
[18] M. Shabanian-Poodeh, R.-A. Hooshmand, M. Shafie-khah, Risk-constrained strategic resilience enhancement of power distribution and natural gas systems through G2P and P2G planning and distributed load Restoration against flood, Sustain. Cities Soc. 112 (2024) 105618, https://doi.org/10.1016/j.scs.2024.105618.
[19] Y. Wang, Y. Yang, Q. Xu, Resilience assessment of the integrated gas and power systems under extreme weather, Energy Rep. 9 (2023) 160–167, https://doi.org/10.1016/j.
[20] A.A. Khan, K. Kubra, M.R. Islam, et al., Microgrid-based operational framework for grid resiliency enhancement: a case study at KUET campus in Bangladesh, Energy Rep. 11 (2024) 1752–1765.
[21] D.K. Mishra, M. Eskandari, M.H. Abbasi, P. Sanjeevikumar, J. Zhang, L. Li, A detailed review of power system resilience enhancement pillars, Electr. Power Syst. Res. 230 (2024) 110223, https://doi.org/10.1016/j.epsr.2024.110223.
[22] R. Uluski, The role of advanced distribution automation in the smart grid. presented at the IEEE PES General Meeting, IEEE, 2010, pp. 1–5.
[23] M.M. Hosseini, M. Parvania, Quantifying impacts of automation on resilience of distribution systems, IET Smart Grid 3 (2) (2020) 144–152.
[24] Y. Xu, Y. Xing, Q. Huang, J. Li, G. Zhang, O. Bamisile, Q. Huang, A review of resilience enhancement strategies in renewable power system under HILP events, Energy Rep. (2023) 200–209, https://doi.org/10.1016/j.egyr.2022.12.128.
[25] C. Chen, J. Wang, F. Qiu, D. Zhao, Resilient distribution system by microgrids formation after natural disasters, IEEE Trans. Smart Grid 7 (2) (2015) 958–966.
[26] A. Abiri-Jahromi, M. Fotuhi-Firuzabad, M. Parvania, M. Mosleh, Optimized sectionalizing switch placement strategy in distribution systems, IEEE Trans. Power Deliv. 27 (1) (2011) 362–370.
[27] S. Heidari, M. Fotuhi-Firuzabad, S. Kazemi, Power distribution network expansion planning considering distribution automation, IEEE Trans. Power Syst. 30 (3) (2014) 1261–1269.
[28] K. Anderson, et al., Quantifying and monetizing renewable energy resiliency, Sustainability 10 (4) (2018) 933.
[29] K. Balasubramaniam, P. Saraf, R. Hadidi, E.B. Makram, Energy management system for enhanced resiliency of microgrids during islanded operation, Electr. Power Syst. Res. 137 (2016) 133–141.
[30] M. Panwar, et al., Integration of flow battery for resilience enhancement of advanced distribution grids, Int. J. Electr. Power Energy Syst. 109 (2019) 314–324.
[31] S. Yao, P. Wang, T. Zhao, Transportable energy storage for more resilient distribution systems with multiple microgrids, IEEE Trans. Smart Grid 10 (3) (2018) 3331–3341.
[32] M. Zare-Bahramabadi, A. Abbaspour, M. Fotuhi-Firuzabad, M. Moeini-Aghtaie, Resilience-based framework for switch placement problem in power distribution systems, IET Gener. Transm. Distrib. 12 (5) (2018) 1223–1230.
[33] M. Nazemi, M. Moeini-Aghtaie, M. Fotuhi-Firuzabad, P. Dehghanian, Energy storage planning for enhanced resilience of power distribution networks against earthquakes, IEEE Trans. Sustain. Energy 11 (2) (2019) 795–806.
[34] E. O. of the President. Council of Economic Advisers: 'Economic benefits of increasing electric grid resilience to weather outages, The Council, 2013.
[35] R. Brown, Cost-benefit analysis of the deployment of utility infrastructure upgrades and storm hardening programs, Quanta Technology, Raleigh, 2009.
[36] J.W. Muhs and M. Parvania, Stochastic spatio-temporal hurricane impact analysis for power grid resilience studies, in: Proceedings of the 2019 IEEE Power & Energy Society Innovative Smart Grid Technologies Conference (ISGT), IEEE, 2019, 1–5.
[37] M. Sadeghian-Jahromi, M. Fotuhi-Firuzabad, S. Fattaheian-Dehkordi, M. Lehtonen, S. Heidari, Investigating the impacts of resiliency of the automation system on distribution network resilience, in: Proceedings of the IEEE PES GTD Int. Conf. Expo. GTD (2023), https://doi.org/10.1109/GTD49768.2023.00028.
[38] P. Georgiou, A.G. Davenport, B. Vickery, Design wind speeds in regions dominated by tropical cyclones, J. Wind Eng. Ind. Aerodyn. 13 (1–3) (1983) 139–152.
[39] J. Kaplan, M. DeMaria, A simple empirical model for predicting the decay of tropical cyclone winds after landfall, J. Appl. Meteorol. Clim. 34 (11) (1995) 2499–2512.
[40] G.J. Holland, An Analytic Model of the Wind and Pressure Profiles in Hurricanes, 1980.
[41] Q. Shi, W. Liu, B. Zeng, H. Hui, F. Li, Enhancing distribution system resilience against extreme weather events: concept review, algorithm summary, and future vision, Int. J. Electr. Power Energy Syst. 138 (2022) 107860.
[42] D. Van Hertem, J. Verboomen, K. Purchala, R. Belmans, W.L. Kling, Usefulness of DC power flow for active power flow analysis with flow controlling devices. in: Proceedings of the Eighth IEE International Conference on AC and DC Power Transmission, IET, 2006, pp. 58–62.
[43] K. Purchala, L. Meeus, D. Van Dommelen, R. Belmans, Usefulness of DC power flow for active power flow analysis, in: in: Proceedings of the IEEE Power Engineering Society General Meeting, 2005, IEEE, 2005, pp. 454–459.
[44] H. Gao, Y. Chen, S. Mei, S. Huang, Y. Xu, Resilience-oriented pre-hurricane resource allocation in distribution systems considering electric buses, Proc. IEEE 105 (7) (2017) 1214–1233.
[45] R.N. Allan, R. Billinton, I. Sjarief, L. Goel, K. So, A reliability test system for educational purposes-basic distribution system data and results, IEEE Trans. Power Syst. 6 (2) (1991) 813–820.
[46] M. Izadi, A. Safdarian, M. Moeini-Aghtaie, M. Lehtonen, Optimal placement of protective and controlling devices in electric power distribution systems: A MIP model, IEEE Access 7 (2019) 122827–122837.
[47] S.M. Schoenung and W.V. Hassenzahl, "Long-vs. short-term energy storage technologies analysis: a life-cycle cost study: a study for the DOE energy storage systems program.," Sandia National Laboratories (SNL), Albuquerque, NM, and Livermore, CA …, 2003.